International Journal of Advanced Computer Science, Vol. 2, No. 11, Pp. 399-411, Nov., 2012.

Unsteady Aerodynamics of Multiple Airfoils in Configuration

Hossain Aziz & Rinku Mukherjee

Manuscript
Received:
3, Jan.,2012
Revised:
26,May, 2012
Accepted:
27,Jul. 2012
Published:
15,Dec., 2012

Keywords
Aerodynamics, Airfoil, Configuration, Unsteady,

***Abstract*— A potential flow model is used to study the unsteady flow past two airfoils in configuration, each of which is suddenly set into motion. The airfoil bound vortices are modeled using lumped vortex elements and the wake behind the airfoil is modeled by discrete vortices. This consists of solving a steady state flow problem at each time-step where unsteadiness is incorporated through the "zero normal flow on a solid surface" boundary condition at every time instant. Additionally, along with the "zero normal flow on a solid surface" boundary condition Kelvin's condition is used to compute the strength of the latest wake vortex shed from the trailing edge of the airfoil. Location of the wake vortices is updated at each time-step to get the wake shape at each time instant. Results are presented to show the effect of airfoil-airfoil interaction and airfoil-wake interaction on the aerodynamic characteristics of each airfoil.**

1. Introduction

The concept of formation flight is not new. It has existed in time when formations were used in the deployment of infantry to concentrate on the backbone of an enemy line. It is however, more commonly attributed to birds and in recent times has gained popularity in lieu of its applicability in various aerospace applications.

Research studies have shown the aerodynamic advantage of birds flying in formation [1] besides providing better visual communication or defense against predators. A bird produces lift by flapping its wings that form a closed loop vortex with wavy vortex lines at the wing tip and spanwise waves generated at every feather tip. Lift is produced by the wing during downstroke and thrust is generated as the wing pivots forward on its axis. During upstroke the wing rotates the humerus about its axis and curves in towards the body. It then rises and extends for the next downstroke [2].

The advantage of flying in formation comes from the existence of rolled-up tip vortices of the leading bird that create upwash on the trailing bird. The leading bird in a formation therefore varies the flow condition of the trailing bird, both temporally and spatially. In other words, a flapping wing in a bird will result in discrete and/or periodic shedding of vortices. This is different from that of fixed aircrafts which shed a continuous sheet of vortices.

Another mode of transportation by over a thousand species of '*miniature*' birds or insects is by flapping their wings. This is in contrast to the flight of large birds like eagles where the flapping of the wings is concentrated to the initial lift-off, landing and stabilization. These large birds primarily "*glide*" with steady fully extended wings which is similar to a traditional wing of an aircraft. Small birds and insects on the other hand continually flap their wings that results in a rapid change in the flow field and such a phenomenon can only be understood by a study of the unsteady aerodynamics of the flow-field [3].

Consequently, both formation flight and insect flight have caught the fancy of modern day researchers with the increase in the possibilities and opportunities of implementing such behavior with traditional aircrafts. Formation flight studies on real aircrafts have shown decrease in induced drag on the trailing aircrafts as well as longer range achievement, which translates into significant fuel savings [4],[5]. These are important developments considering that cargo freight is increasing by the minute. Especially, the long-range freights will be the order of the day in 10 years time. Hence, fuel consumption is an important consideration and formation flight could provide some answers. Defence applications are ample as well like the use of multi-UAVs in formation for surveillance purposes will increase their endurance.

Taking a cue from insect flight, creation of micro-UAVs has opened up yet another field for researchers to focus. Such vehicles are designed for very small payloads for remote-sensing operations where access is limited due to various hazards.

Computational implementation of these phenomena involves a numerical representation of the lifting surface as well as the wake behind the lifting surface. In case of unsteady formation flight vortex-vortex as well as vortex-solid boundary interactions are taken into account.

Bowles and Smith [6] studied the flow past nearly aligned configurations of multiple successive blades inducing lift. Here, a blade is oriented centrally to the incumbent wake from a preceding blade. Each blade is subjected to a combination of separated unsteady boundary layers with fixed wake displacement. The authors report stream-wise jumps in the pressure, velocity and mass flux

This work was partly supported by the Aeronautical Research and Development Board, Bangalore, India.

Hossain Aziz (Project Officer) and Rinku Mukherjee (Assistant Professor) are with Indian Institute of Technology Madras, Chennai, Department of Applied Mechanics. (hossainaziz@gmail.com; riinku@iitm.ac.in)

from the leading edge of each blade.

Fanjoy and Dorney [7] studied the tandem-airfoil interactions in different regimes using computational methods. A two dimensional tandem airfoil geometry comprising two NACA airfoils was tested at subsonic and sonic speeds. The results showed that, at positive angles of attack, the lift/drag ratio of the lead airfoil is increased while the trailing airfoil experiences less lift and drag, due to reduced local angle of attack.

Zannetti, Gallizio and Ottino [8] analytically addressed the unsteady two dimensional rotational flow past doubly connected domains. Flow was modelled as a potential flow with point singularities, by concentrating the vorticity in point vortices. The dependence of complex potential on time was defined according to Kelvin's theorem. Vortex shedding and time evolution of circulation past a two-element airfoil and past a two-bladed Darrieus turbine was studied as physical examples.

Husain, Abdullah and Yap [9] did a two-dimensional analysis of tandem/staggered arranged airfoils of the canard and wing of an Eagle 150 aircraft using computational fluid dynamics and also conducted aerodynamic tests in an open-circuit wind tunnel.

The wind tunnel experiments for the tandem/staggered positions of the airfoils gave the optimum position for the wing and were validated by simulation. It was also observed in the simulation results that with the tandem position, the wake created by the leading airfoil disturbs the inflow at the trailing airfoil.

The current work is motivated by the prospect of combining the advantages of both formation flight and insect flight. In other words, unsteady aerodynamics of a formation flight. Some practical examples are that of the unsteady motion of rotorcrafts, aircrafts with multiple lifting surfaces like wing-canard and wing-tail configurations, multi-bladed vertical axis wind turbines, industrial mixers, turbine blades, food mixers, blenders, grinders etc.

In this paper, a two-dimensional unsteady analysis by extending a potential-flow approach using a discrete vortex method, of unsteady flow past two airfoils suddenly set into motion is presented. The effect of airfoil-airfoil interaction and airfoil-wake interaction on the aerodynamic characteristics of each airfoil is studied.

2. Numerical Procedure

The current numerical method consists of extending an unsteady analysis of a single airfoil and its wake using discrete vortices [10] to include multiple airfoils and hence multiple wakes. The airfoils are simulated using a discrete lumped vortex model and the time-dependant wakes are simulated using trailing edge discrete vortices shed at every time-step. The flow field is force-free, i.e. the strength of the wake vortices shed from the airfoils remains unchanged. A time-stepping method is used to update the location of these vortices and hence predict the individual wake shape. A vortex core [11] approach is used for predicting the wake shape of a single airfoil that prevents any singularities in the conservative flow field when the free vortices interact with each other and smooth vortex roll-up is obtained. This approach is extended to the current analysis consisting of multiple wakes. In addition to multiple wakes, the flow field also consists of multiple airfoils and an additional condition for near-field vortex-solid surface interaction is introduced to account for vortex dissipation when the free vortices interact with the solid airfoil surfaces.

A. Governing Equations

Potential flow past two airfoils in configuration is considered for which the Laplace equation is the governing equation. However, the problem considered is unsteady and the Laplace equation is devoid of any time considerations. Hence, unsteadiness is introduced into the problem through the "zero-normal flow on a solid surface" boundary condition as given in Equ. 1.

B. Boundary Conditions and Influence Coefficients

Boundary conditions imposed are the "zero-normal flow on a solid surface" boundary condition given in (1) and the Kelvin condition given in (2) for each airfoil in configuration. Both these conditions are used in tandem at every time instant to generate the $(2N+2)\times(2N+2)$ influence coefficient matrix for two airfoils in configuration. Finally, a matrix equation given in (3) is solved at every time instant for the strength of the bound vortices of each airfoil (Γ_N) in the configuration and the strength of the wake vortices shed from each airfoil ($\Gamma_{W,t}$). The subscript t denotes the latest time step.

$$(\nabla\Phi + U_\infty).\hat{n} = 0; \quad \hat{n} = \hat{n}(X,Y,Z,t) \qquad \text{(Equ. 1)}$$

$$\frac{d\Gamma}{dt} = 0 \qquad \text{(Equ. 2)}$$

$$\begin{bmatrix} F1 & F2 & F3 & F4 \\ G1 & G2 & G3 & G4 \\ L1 & L2 & L3 & L4 \\ M1 & M2 & M3 & M4 \end{bmatrix} \begin{bmatrix} \Gamma_A \\ \Gamma_B \\ \Gamma_{WA} \\ \Gamma_{WB} \end{bmatrix} = \begin{bmatrix} rhs_A \\ rhs_B \\ -(\Gamma_{WA,1} + \Gamma_{WA,2} + ... + \Gamma_{WA,t-1}) \\ -(\Gamma_{WB,1} + \Gamma_{WB,2} + ... + \Gamma_{WB,t-1}) \end{bmatrix} \qquad \text{(Equ. 3)}$$

Where,

$$F1 = \begin{bmatrix} f_{1,1} & : & f_{1,N} \\ : & : & : \\ : & : & : \\ f_{N,1} & : & f_{N,N} \end{bmatrix}_{N\times N} \qquad F2 = \begin{bmatrix} f_{1,N+1} & : & f_{1,2N} \\ : & : & : \\ : & : & : \\ f_{N,1} & : & f_{N,2N} \end{bmatrix}_{N\times N}$$

$$G1 = \begin{bmatrix} f_{N+1,1} & : & f_{N+1,N} \\ : & : & : \\ : & : & : \\ f_{2N,1} & : & f_{2N,N} \end{bmatrix}_{N\times N} \qquad G2 = \begin{bmatrix} f_{N+1,N+1} & : & f_{N+1,2N} \\ : & : & : \\ : & : & : \\ f_{2N.N+1} & : & f_{2N.2N} \end{bmatrix}_{N\times N}$$

$$\Gamma_A = \begin{bmatrix} \Gamma_1 \\ : \\ \Gamma_N \end{bmatrix}_{N\times 1} \qquad \Gamma_B = \begin{bmatrix} \Gamma_{N+1} \\ : \\ \Gamma_{2N} \end{bmatrix}_{N\times 1} \qquad F3 = \begin{bmatrix} f_{1,2N+1} \\ : \\ f_{N,2N+1} \end{bmatrix}_{N\times 1}$$

$$F4 = \begin{bmatrix} f_{1,2N+2} \\ : \\ f_{N,2N+2} \end{bmatrix}_{N\times 1} \quad G3 = \begin{bmatrix} g_{N+1,2N+1} \\ : \\ g_{2N,2N+1} \end{bmatrix}_{N\times 1} \quad G4 = \begin{bmatrix} g_{N+1,2N+2} \\ : \\ g_{2N,2N+2} \end{bmatrix}_{N\times 1}$$

$$\Gamma_{WA} = \left[\Gamma_{WA,t}\right]_{1\times 1} \quad \Gamma_{WA} = \left[\Gamma_{WB,t}\right]_{1\times 1} \quad L1 = M2 = \left[1\cdots\cdots 1\right]_{1\times N}$$

$$L2 = M1 = \left[0\cdots\cdots 0\right]_{1\times N} \quad L3 = M4 = \left[1\right]_{1\times 1} \quad L4 = M3 = \left[0\right]_{1\times 1}$$

$F1\Gamma_A$ is the influence of the bound vortices of airfoil A on itself. $F2\Gamma_B$ is the influence of the bound vortices of airfoil B on airfoil A. $G1\Gamma_A$ is the influence of the bound vortices of airfoil A on airfoil B. $G2\Gamma_B$ is the influence of the bound vortices of airfoil B on itself. Γ_{WA} and Γ_{WB} are the strengths of the latest shed trailing vortices from airfoil A and B respectively. $F3\Gamma_{WA}$ is the influence of the latest shed trailing vortex from airfoil A on airfoil A. $F4\Gamma_{WB}$ is the influence of the latest shed trailing vortex from airfoil B on airfoil A. $G3\Gamma_{WA}$ is the influence of the latest shed trailing vortex from airfoil A on airfoil B. $G4\Gamma_{WB}$ is the influence of the latest shed trailing vortex from airfoil B on airfoil B. The first two rows of the influence coefficient matrix are a statement of the zero-normal flow boundary condition on both the airfoils. The last two rows of the influence coefficient matrix are a statement of the Kelvin condition on both the airfoils individually.

C. Near-Field Vortex-Solid Surface Interaction

As time progresses the free vortices shed into the wake travel and change their original locations. A time-stepping method is used to update the location of the shed vortices at the end of each time step. In the current problem since multiple airfoils are present in the flow field, the trailing airfoil interacts with the wake vortices of the leading airfoil. It was observed by Fage and Johansen [12] that vortices which approach too close to the surface of a plate, dissipate by the action of viscosity. This phenomenon was also observed by Nakagawa [13]. In the present work, this effect is taken into account whenever the following condition in encountered:

$$r \le 0.08c \qquad \text{(Equ. 4)}$$

Where r is the distance between a free vortex in the flow field and a solid surface.

Whenever a wake vortex satisfies this condition, its influence on the flow-field, i.e. the velocity induced due to it on the bound vortices and the wake vortices and wake shape is ignored since it is considered "dissipated". The strength of this vortex is however continued to be used to satisfy the Kelvin condition even after this condition is met as the flow-field is considered to be force-free and the net vorticity of the flow-field remains constant.

D. Near-Field Vortex-Vortex Interaction

For the condition when there are several free vortices in the flow field and they interact with each other, the stream function criteria suggested by Chorin [11] is used as given in Equ. 5. This prevents any infinite velocities due to two vortices coming too close to each other.

$$\psi_\sigma = \begin{cases} \dfrac{\Gamma \log r}{2\pi} & r > \sigma \\ \dfrac{\Gamma \log\left(\dfrac{r}{\sigma}\right)}{2\pi} & r \le \sigma \end{cases} \qquad \text{(Equ. 5)}$$

In the current work, $\sigma = 0.08c$, where r is the distance between two free vortices and σ the radius of the core scooped out about the free vortex.

3. Results

Results are presented for a configuration consisting of two airfoils as shown in Figure 1. The leading airfoil is denoted as **A** and the trailing airfoil is denoted as **B**.

A fixed reference frame, **(X, Y)** is attached to airfoil **A** and the origin, **O(0, 0)** of this reference frame is located at the leading edge of airfoil **A**. A moving reference frame, **(x,y)** is attached to the trailing airfoil **B** and the origin of this reference frame **o(X0, Y0)** is located at the leading edge of airfoil **B**. Note that **X0** and **Y0** are calculated with respect to the fixed reference frame, (**X, Y).**

The results presented in this paper are validated with experiment and numerical results in literature and presented in section *A*. The lift coefficient for the configuration over non-dimensionalised time is validated with the analytical results of Wagner [14], the wake shape of each airfoil in the configuration is validated with the experimental and numerical results of Katz [15] and interactions of airfoils and wake are validated with the numerical results of Platzer [16]. Following the validation, a comparative study of a single airfoil and two airfoils in configuration is presented along with three case studies showing the effect on the aerodynamic characteristics due to both temporal and spatial changes in the configuration. Temporal changes are incorporated by changing the angle of attack of airfoil A and the spatial changes are incorporated by changing the relative position of the airfoils with respect to each other. Results are presented for coefficients of lift, $C_l(t)$, pitching moment about the leading edge of the respective airfoils, $C_m(t)$, induced drag, $C_d(t)$ and wake shape of both airfoils.

A. Validation

Two NACA0012 airfoils, each of chord length c=1 are considered for the configuration as shown in Fig. 1.

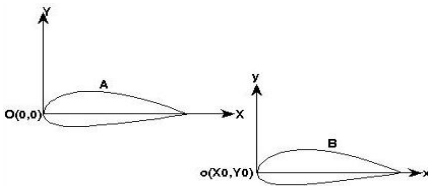

Fig. 1 Schematic diagram of airfoils in configuration

1) Validation of $C_l(t)$: The results from the current work on $C_l(t)$ are compared with the analytical results for the same of Wagner [14]. However, Wagner's result is for a single airfoil in comparison to the present results, which are for a configuration shown in Fig. 2. Hence, for validation purposes, the distance between the two airfoils is taken as 50c in the present analysis. It is expected that at such a large distance, the influence of the airfoil bound vortices and the wake vortices on each other will be minimal. Each airfoil is at an angle of attack of 5 degrees, which is the same for both the present results and that of Wagner.

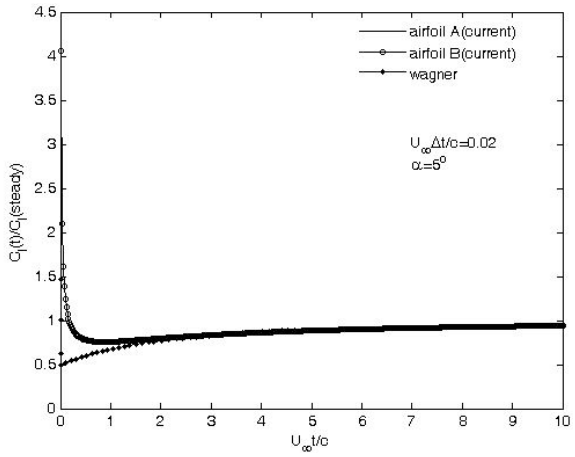

Fig. 2 $C_l(t)$ of airfoils A & B for (X0, Y0) ≈ (50c, 0)

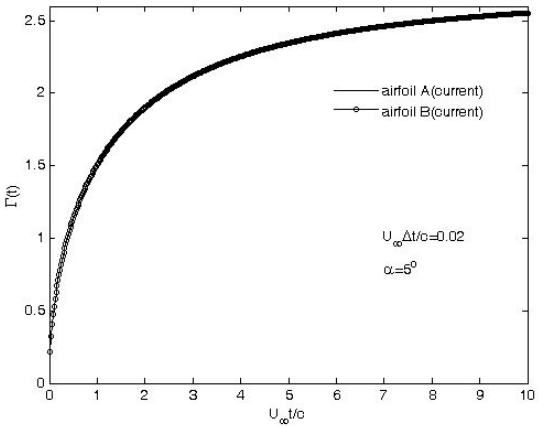

Fig. 3 $\Gamma(t)$ of airfoils A & B for (X0, Y0) ≈ (50c, 0)

The plot of $C_l(t)/C_l(steady)$ vs non-dimensionalised time, $U_\infty t/c$ for both airfoils is shown in Figure 2. The results are compared with the analytical results for the same of Wagner [14]. It can be seen from Figure 2, that the $C_l(t)/C_l(steady)$ values of both airfoils exactly match each other and the comparison with the analytical result is also good.

There is however, some disagreement of the current result with that of Wagner at very small time steps, e.g. $U_\infty t/c \le 1$. This may be attributed to the loss in accuracy due to the numerical approach used in this work for the computation as decreasing the time-step does not improve the result. This problem is not expected in an analytical approach.

Fig. 3 shows the circulation distribution, $\Gamma(t)$ vs $U_\infty t/c$ for both airfoils. Here too as expected the result shows that both airfoils are unaffected by the presence of each other.

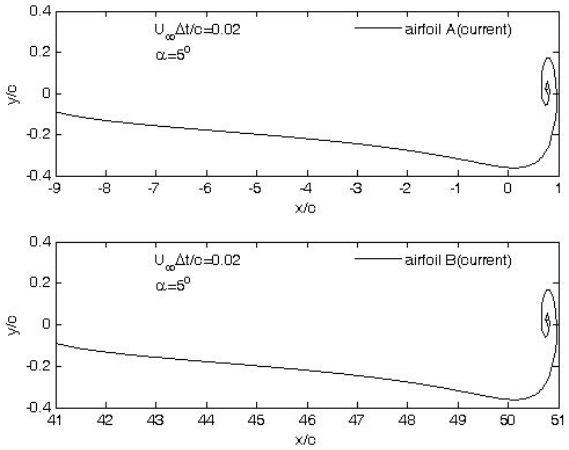

Fig. 4 Wake shape of airfoils A & B for $(X_0, Y_0) \approx (50, 0)$

Figure 4 shows the vortex roll up for for both the airfoils. As expected, the wake shape due to the roll-up of the vortices shed from each airfoil is also not affected by the presence of the other bound vortices or wake vortices. Results for the circulation and wake shape were not available from Wagner [14] for comparison.

2) Validation of Wake Shape: Wake shape of both the airfoils, calculated using the present numerical method are compared with the computational and experimental results of Katz and Weihs [15]. In this case too the results of Katz and Weihs are for a single airfoil. Hence, in the current analysis, the distance between the two airfoils in configuration is taken as 100c. It is expected that at such a large distance, the influence of the airfoil bound vortices and the wake vortices on each other will be minimal. As in the analysis of Katz and Weihs, to validate the wake shape of the present analysis, the configuration of two NACA0012 airfoils as shown in Fig. 1 is subjected to heaving motion. The parameters of heaving motion are:

$$\frac{\omega c}{2U_\infty} = 8.5; \quad \frac{U_\infty}{c} = 1.56/s; \quad \frac{h_0}{c} = 0.019; \quad \omega = 4.26 \times 2\pi\, rad/s$$

The experimental and numerical results of Katz and Weihs are shown in Fig. 5. The results for the wake shape from the current analysis are shown in Fig. 6.

It can been seen that there is no interaction between the airfoil bound vortices and wake vortices due to the 100c distance between them and hence the wake shape of both airfoils are not different from each other. From Figs. 5 and 6 it is also observed that wake shape of the heaving airfoils from the present study are in good agreement with the experimental and computational results of Katz and Weihs [15].

(a)

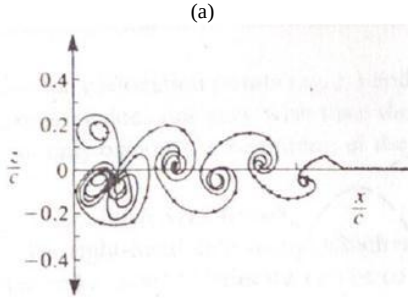

(b)

Fig. 5 Wake shape of a heaving airfoil from Katz and Weihs [15] (a) experimental (b) computational.

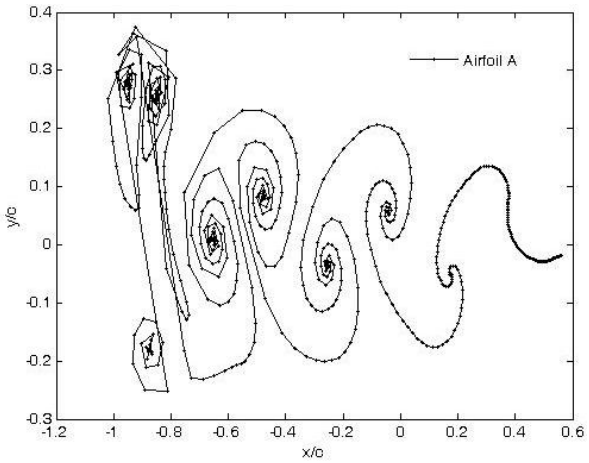

(a)

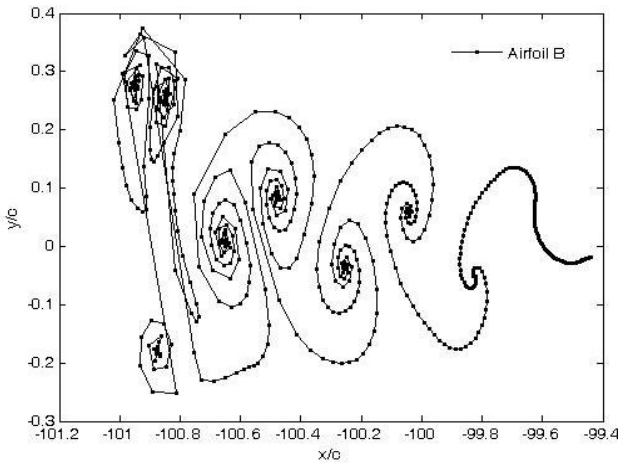

(b)

Fig. 6. Wake shape of heaving airfoils A and B from present study

3) Validation of Airfoil and Wake Interaction: A comparison between the results from the present study and the computational results of Platzer [16] for airfoil and wake interaction is presented here. For a configuration of two NACA0012 airfoils, $(X_0, Y_0) = (0.5c, 0.2c)$, Platzer's numerical code could not account for the interaction of the vortices shed from the leading airfoil with the trailing airfoil surface for such minimal distances. They had to therfore adjust the configuration in such a way that the vortices do interact but they do not come close enough to induce infinite velocities in the numerical solution. Hence, they used the configuration $(X_0, Y_0) = (1.5c, 0.2c)$, where the airfoils are also undergoing a step change in angle of attack from 0^o to 5^o. The results for this configuration without the step change in angle of attack is generated with the present code and presented in Fig. 7. The results show individual cases of different angles of attack for the airfoils in configuration. The present numerical scheme accounts for the interaction of vortices with solid airfoil surfaces as well as with each other at minimal distances without inducing any infinite velocities in the flow-field.

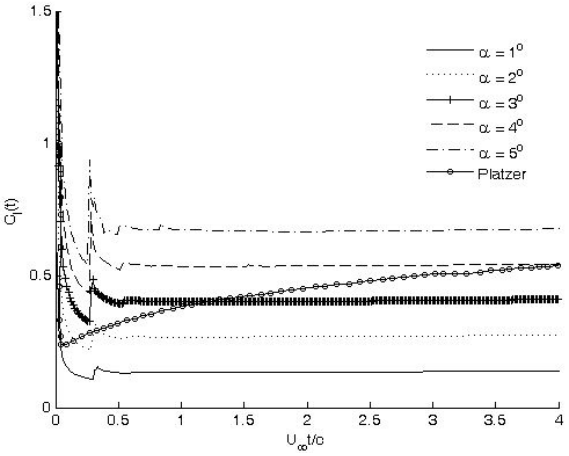

(a)

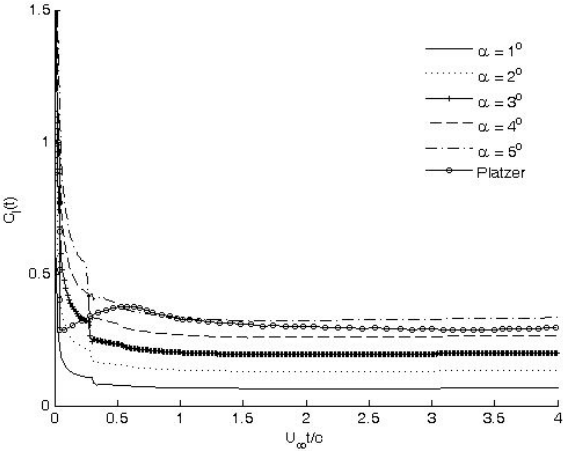

(b)

Fig. 7 $C_l(t)$ for (a) airfoil A (b) airfoil B

The abrupt changes in $C_l(t)$ in the results of the current work are explained in more detail in following sections. Platzer's results are similar to that of a single airfoil case of Wagner and non-interacting results from the present study shown in Fig. 2. It is therefore safe to say that

the present code is robust and can account for vortex interactions for any given configuration.

B. Single Airfoil and Configuration of Two Airfoils: A Comparative Study

Since the flow field around a single airfoil is different when it is in a configuration with another airfoil (e.g. airfoils A & B as shown in Fig. 1), it is expected that there will be differences in their aerodynamic characteristics as well. Hence, a comparison of the same is presented here. For the airfoils in configuration, the physical offset X_o=2c and Y_o=0, both airfoils are at an angle of attack of 4° and both airfoils are travelling at a velocity of 27m/s. The single airfoil is at an angle of attack of 4° and travelling at a velocity of 27m/s.

Fig. 8 shows the plot of $C_l(t)$ vs $U_\infty t/c$. It is observed that around $U_\infty t/c \approx 1$, there are sharp changes in the $C_l(t)$s of both airfoils in the configuration unlike the airfoil operating alone.

Leading up to $U_\infty t/c \approx 1$, after the initial sharp drop just after the airfoils are set into sudden motion, the $C_l(t)$s of both airfoils increase smoothly. The increase in $C_l(t)$ for airfoil A is only slightly more than the single airfoil and can be attributed to the upwash created on it by the bound vortices of airfoil B. For airfoil B, on the other hand, the increase in $C_l(t)$ can be attributed to the upwash produced on it by the trailing edge vortex shed by airfoil A.

At $U_\infty t/c \approx 1$, the strong trailing edge vortex from airfoil A moves more downstream and when it just crosses the leading edge of airfoil B it causes a strong downwash on airfoil B resulting in a sharp decease in its $C_l(t)$. Similarly, the downwash created by this vortex on airfoil A decreases which causes a sudden increase in the $C_l(t)$ of airfoil A. Hence, the strength of the trailing edge vortices from airfoil A completely overrides the strength of the bound vortices in the vicinity.

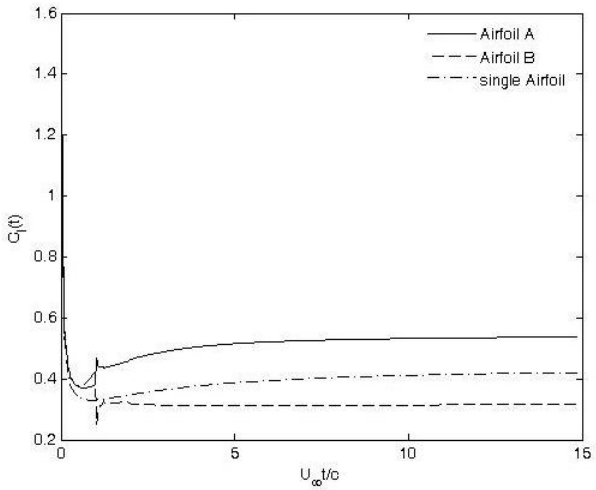

Fig. 8 $C_l(t)$ of an airfoil operating by itself and in configuration

For $U_\infty t/c > 1$, the $C_l(t)$ of airfoil B is higher than that of airfoil A. This can be attributed to the fact that the effect of the trailing vortices of both airfoils becomes weaker and the effect of the bound vortices dominates. Hence, the aerodynamic characteristics are dominated by the effect of the bound vortices. As a result, the leading airfoil A causes downwash on the trailing airfoil B which in turn causes the $C_l(t)$ of airfoil B to be less than that of the single airfoil. The bound vortices of airfoil B cause upwash on airfoil A, which in turn causes the $C_l(t)$ of airfoil A to be higher than that of the single airfoil. Clearly, the strength of the trailing edge vortices from airfoil A is stronger than the strength of the bound vortices of airfoil B.

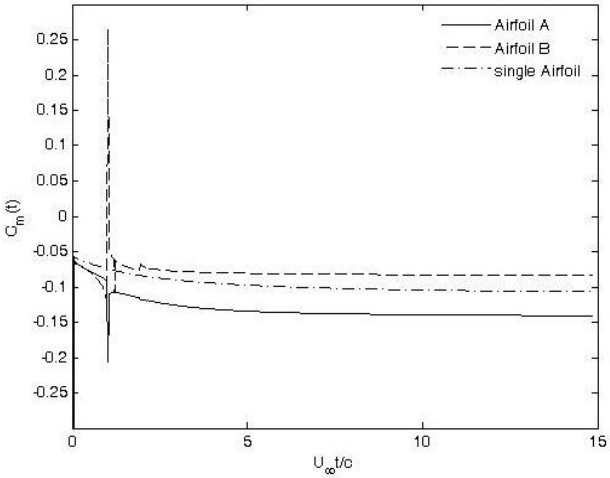

Fig. 9 $C_m(t)$ of an airfoil operating by itself and in configuration

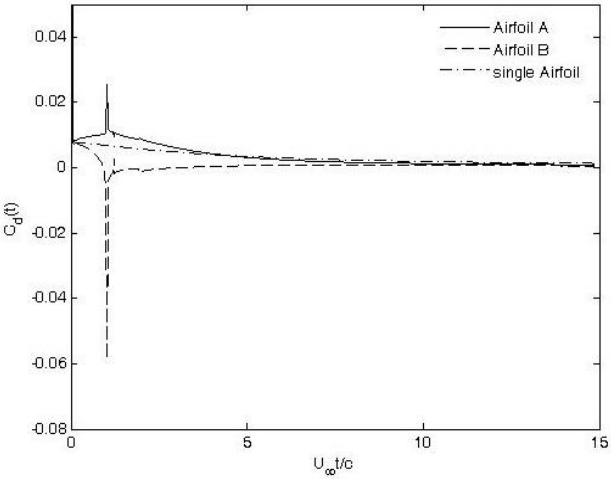

Fig. 10 $C_d(t)$ of an airfoil operating by itself and in configuration

Fig. 9, 10 and 11 show the plots of $C_m(t)$, $C_d(t)$ and wake shape vs $U_\infty t/c$ for both airfoils respectively. It is seen from Fig. 9 that the $C_m(t)$ of airfoil A is less than that of airfoil B after $U_\infty t/c \approx 1$. This is exactly reversed compared to the $C_l(t)$ plot and is expected.

From Fig. 7 it is seen that the induced drag coefficient, $C_d(t)$ of both the airfoils in configuration is dominated by the trailing edge vortices and after a certain time it trails off to zero and matches the result for the single airfoil as these trailing edge vortices move downstream and their

dominance decreases.

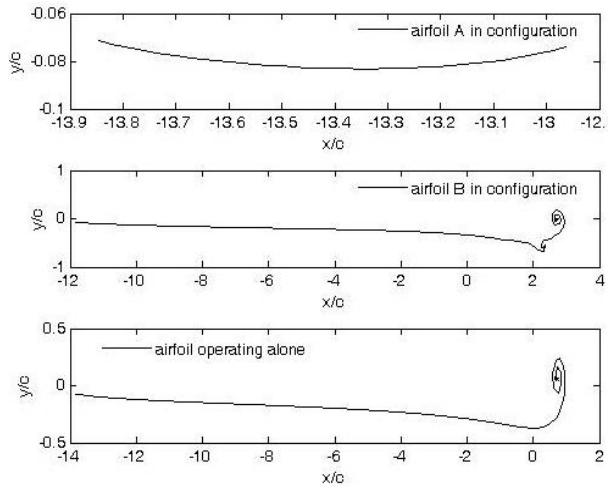

Fig. 11 Wake shape of an airfoil operating by itself and in configuration

From Fig. 11 it is seen that there is no vortex roll-up for airfoil A but there is significant roll-up for airfoil B as well as the single airfoil. For airfoil B, there is also a secondary vortex roll-up, which can be attributed to additional vorticity in the wake of airfoil B due to the trailing edge vortices of airfoil A.

C. Case Study 1: Effect of Varying X_o

The effect of varying the physical offset X_o (as shown in Fig. 1) on the aerodynamic characteristics of two airfoils in configuration (airfoils A & B as shown in Fig. 1) is presented here.

The physical offset Y_o=0, both airfoils are at an angle of attack of 4° and both airfoils are travelling at a velocity of 27m/s.

Fig. 12 shows the variation of $C_l(t)$ with $U_\infty t/c$ for different values of X_o (the X-location of the leading edge of the trailing airfoil B) for airfoils A and B. For both airfoils, there are some sharp changes in $C_l(t)$, the occurrence of which is delayed with the increase in X_o. It is seen that with the increase in X_o, there is a decrease in $C_l(t)$ of the leading airfoil A post the occurrence of the sharp changes as shown in Fig. 12(a). This behaviour is reversed for the trailing airfoil B as shown in Fig. 12(b).

Before the occurrence of the sharp changes, for both airfoils with increase in X_o there is a decrease in $C_l(t)$.

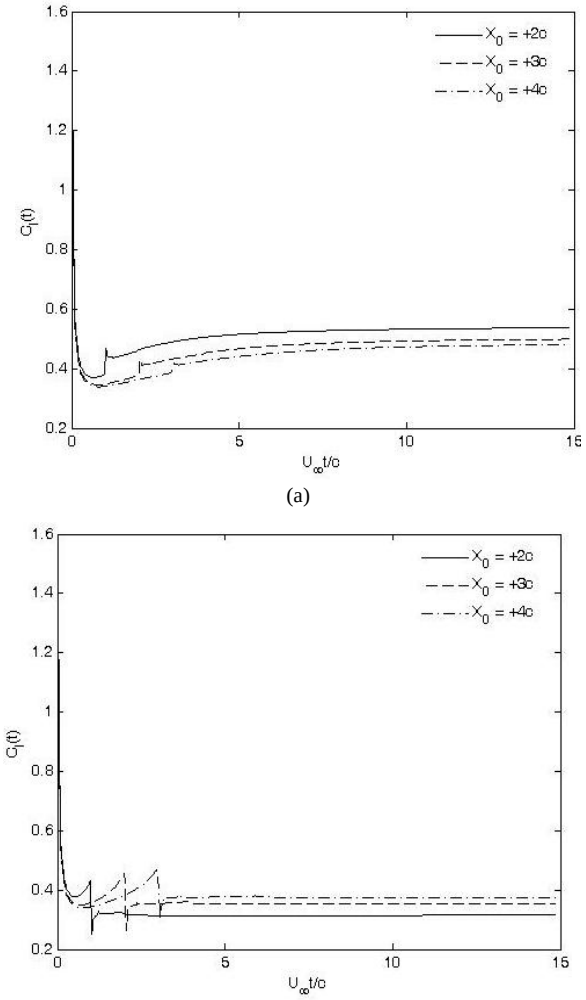

Fig. 12 $C_l(t)$ for $Y_0 = 0$, $\alpha_A = \alpha_B = 4^o$, $V_A = V_B = 27$m/s (a) airfoil A and (b) airfoil B

Such behaviour can be attributed to the very high strength of the initial vortex shed from the trailing edge of each airfoil and its effect on the configuration decreasing with time. The location of the peaks can be said to be the time when the trailing edge vortex from the leading airfoil A crosses the leading edge of the trailing airfoil B. This phenomenon is explained in detail in section *B.*

In this case, an increase in X_o means that the trailing vortex from airfoil A has to travel longer to cross the trailing airfoil B. Hence, the occurrence of the peak is delayed with increase in X_o.

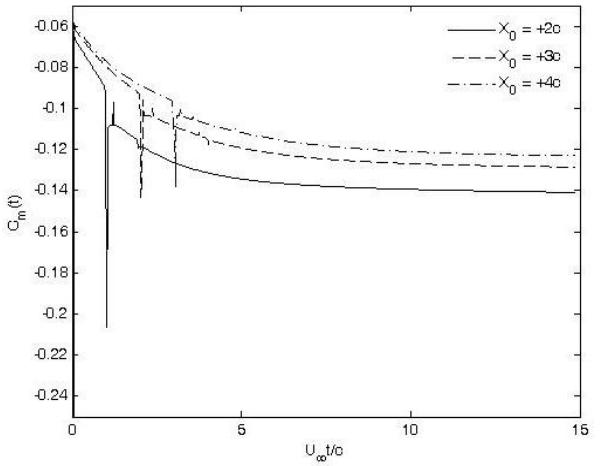

(a)

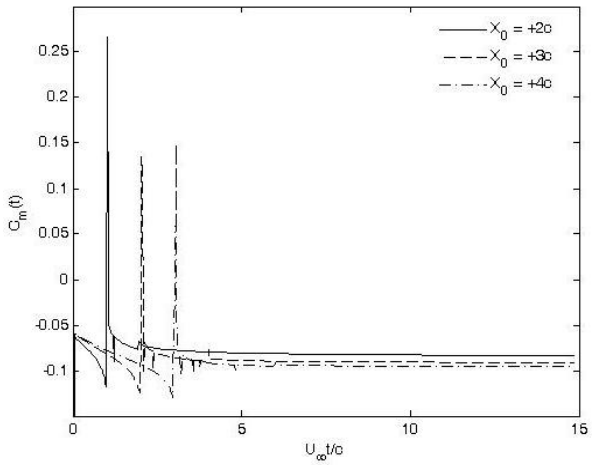

(b)

Fig. 13 $C_m(t)$ for $Y_0 = 0$, $\alpha_A = \alpha_B = 4^o$, $V_A = V_B = 27$m/s (a) airfoil A and (b) airfoil B

Figs. 13, 14 and 15 show the plots of $C_m(t)$, $C_d(t)$ and wake shape vs $U_\infty t/c$ for both airfoils respectively. It is seen that the sharp peaks in the $C_l(t)$ plots are repeated in the $C_m(t)$ and $C_d(t)$ plots as well and this is expected. The nature of the peaks in the $C_m(t)$ plots is the reverse and the nature of the peaks in the $C_d(t)$ plots is the same as that of the $C_l(t)$ plots and this is expected. It is interesting to note the development of very sharp negative $C_d(t)$ on the trailing airfoil B before it trails off and becomes zero.

No significant roll-up of the vortices shed from the leading airfoil **A** is observed but significant roll-up is obtained for the trailing airfoil **B**. This indicates that the wake of the leading airfoil is significantly affected by the presence of the trailing airfoil.

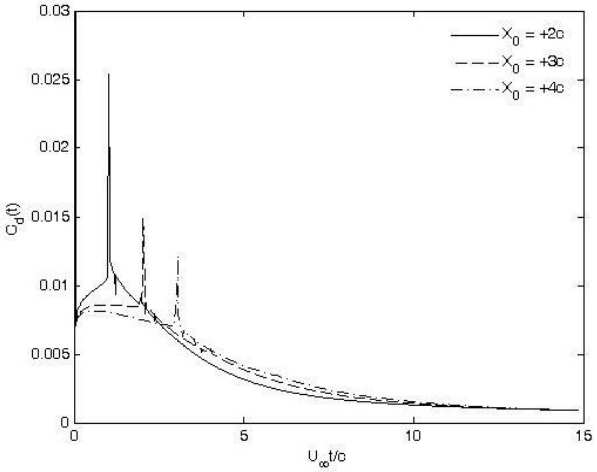

(a)

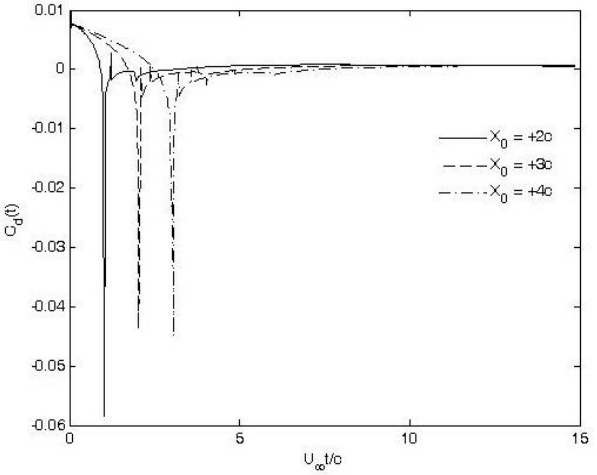

(b)

Fig. 14 $C_d(t)$ for $Y_0 = 0$, $\alpha_A = \alpha_B = 4^o$, $V_A = V_B = 27$m/s (a) airfoil A and (b) airfoil B

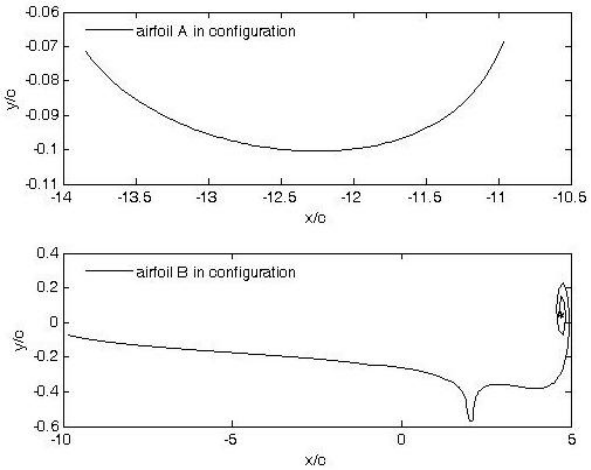

Fig. 15 Wake shape when $(X_0, Y_0) = (4c, 0)$ $\alpha_A = \alpha_B = 4^o$, $V_A = V_B = 27$m/s

D. Case Study 2: Effect of Varying Y_o

The effect of varying the physical offset Y_o (as shown in Fig. 1) on the aerodynamic characteristics of two airfoils in configuration (airfoils A & B as shown in Fig. 1) is

presented here.

The physical offset X_o=2c, both airfoils are at an angle of attack of 4° and both airfoils are travelling at a velocity of 27m/s.

Fig. 16 shows the variation of $C_l(t)$ with $U_\infty t/c$ for different values of Y_o (the Y-location of the leading edge of the trailing airfoil B) for airfoils A and B. It is seen in Fig. 16(a) that there are some sharp changes in the $C_l(t)$ of airfoil A while the $C_l(t)$ of airfoil B as shown in Fig. 16(b) is devoid of any major peaks. The presence of the peaks in the $C_l(t)$ of airfoil A can be attributed to the dominance of a very strong trailing vortex, the effect of which decreases with increase in the Y-offset and also as it moves downstream with time.

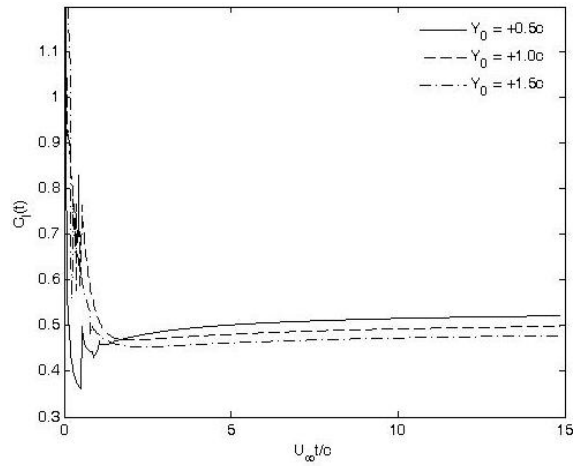

(a)

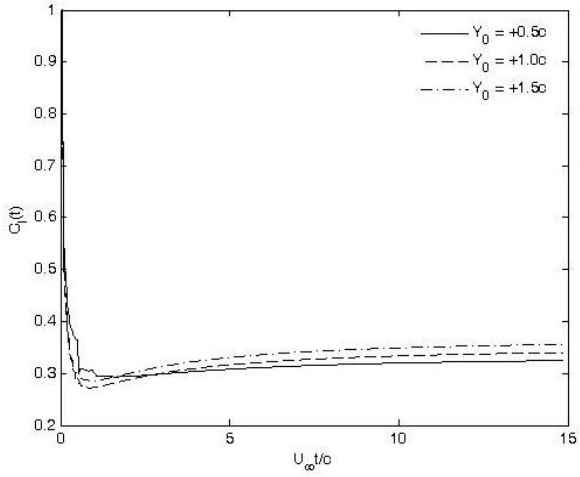

(b)

Fig. 16 $C_l(t)$ for X_0 = 2c, $\alpha_A = \alpha_B = 4^o$, $V_A = V_B$=27m/s (a) airfoil A and (b) airfoil B

The absence of such peaks in the $C_l(t)$ of airfoil B is due to its Y-offset from airfoil A as a result of which the effect of the wake vortices is minimized.

Figs. 17, 18 and 19 show the plots of $C_m(t)$, $C_d(t)$ and wake shape vs $U_\infty t/c$ for both airfoils respectively.

It is seen that the $C_m(t)$ and $C_d(t)$ plots consist of sharp peaks as well and this is expected.

No significant roll-up of the vortices shed from the leading airfoil **A** is observed but some roll-up is obtained for the trailing airfoil **B** as seen in Fig. 19.

This indicates that the wake of the leading airfoil is affected by the presence of the trailing airfoil. However, in this case the bound vortices take precedence over the trailing vortices.

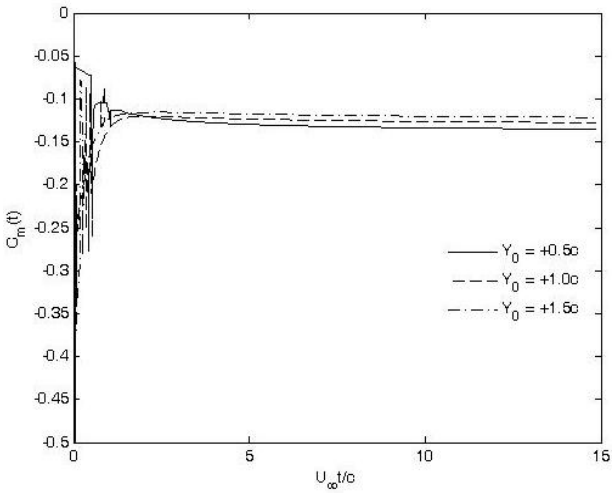

(a)

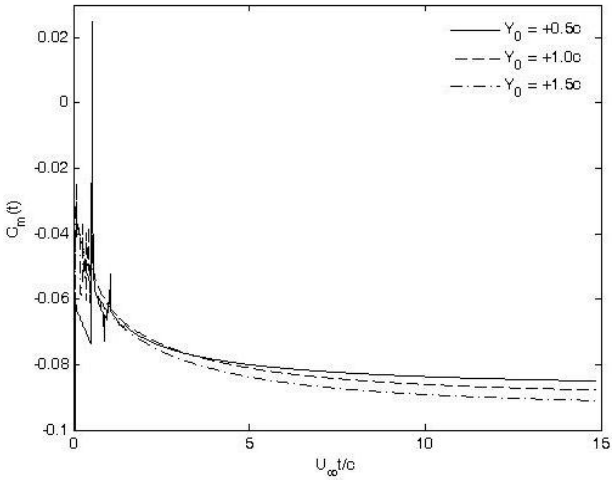

(b)

Fig. 17 $C_m(t)$ for X_0 = 2c, $\alpha_A = \alpha_B = 4^o$, $V_A = V_B$=27m/s (a) airfoil A and (b) airfoil B

*E. Case Study 3: Effect of Varying α_A, i.e. Angle of Attack of Airfoil **A***

The effect of making a temporal change in the aerodynamic characteristics of the two airfoils in configuration (airfoils A & B as shown in Fig. 1) is obtained by varying the leading airfoil (airfoil A as shown in Fig. 1) angle of attack, α_A. The results are presented here. The physical offsets X_o=2c, and Y_o=0, airfoil B is at an angle of attack of 4° and both airfoils are travelling at a velocity of 27m/s.

Fig. 20 shows the variation of $C_l(t)$ with $U_\infty t/c$ for different values of α_A (the angle of attack of airfoil A) for airfoils A and B.

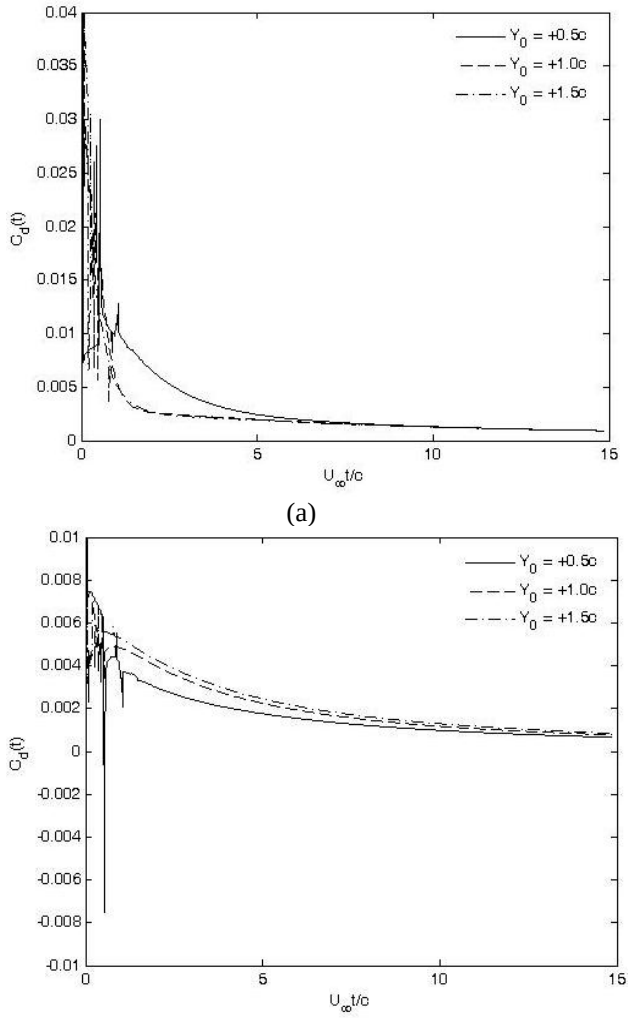

Fig. 18 $C_d(t)$ for X_0 = 2c, $\alpha_A = \alpha_B = 4^o$, $V_A = V_B$=27m/s (a) airfoil A and (b) airfoil B

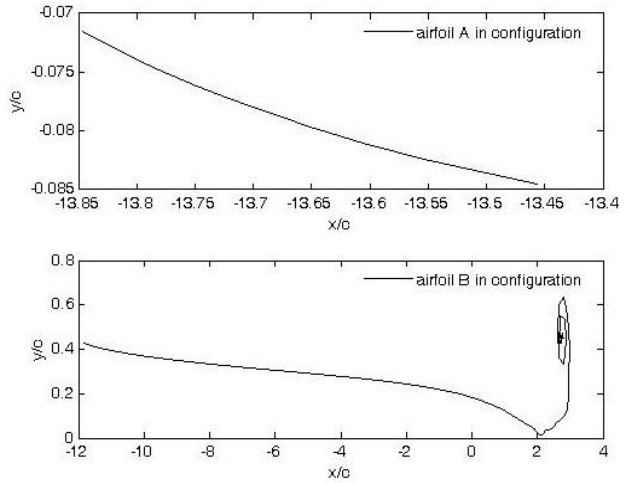

Fig. 19: Wake shape when (X_0, Y_0) = (2c, 0.5c) $\alpha_A = \alpha_B = 4^o$, $V_A = V_B$=27m/s

Here the Y-offset of the trailing airfoil is zero and the X-offset is 2c, which is not very large. Hence, the effect of the trailing edge vortices finds prominence for both airfoils. Sharp changes in $C_l(t)$ are observed for both airfoils. The time of occurrence of these peaks is not affected by the change in α_A as is seen from Fig. 20. Prior to the occurrence of the peaks, the $C_l(t)$ increases with increase in α_A for both airfoils. Post occurrence of the peaks this behaviour is maintained for the leading airfoil A but is reversed for the trailing airfoil B. This can be attributed to the very strong trailing edge vortices, the effect of which decreases with time.

Clearly, the strength of the trailing edge vortex of the leading airfoil A increases with the increase in its angle of attack α_A.

Figs. 21, 22 and 23 show the plots of $C_m(t)$, $C_d(t)$ and wake shape vs $U_\infty t/c$ for both airfoils respectively.

It is seen from Figs. 21 and 22 that the sharp peaks are also present for the $C_m(t)$ and $C_d(t)$ plots. The nature of the peaks for the $C_m(t)$ plots is opposite and the nature of the $C_d(t)$ plots is similar to that of the $C_l(t)$ plots. This is expected.

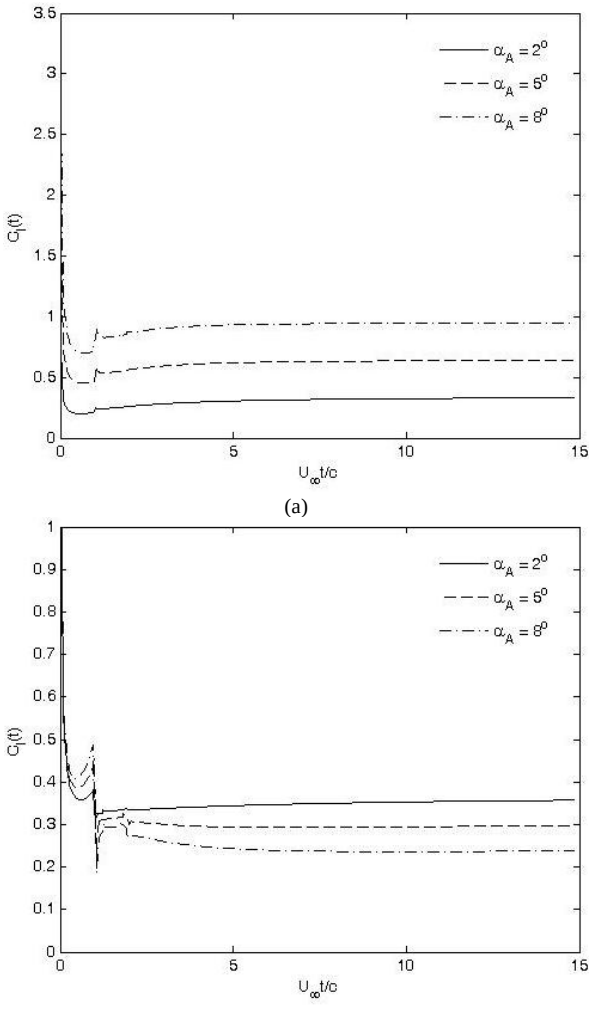

Fig. 20 $C_l(t)$ for (X_0, Y_0) = (2c, 0), $V_A = V_B$=27m/s, $\alpha_B = 4^o$ (a) airfoil A and (b) airfoil B

There is a sharp negative drag for the trailing airfoil as shown in Fig. 22(b) and the sharpness increases with the increase in the angle of attack of the leading airfoil, α_A.

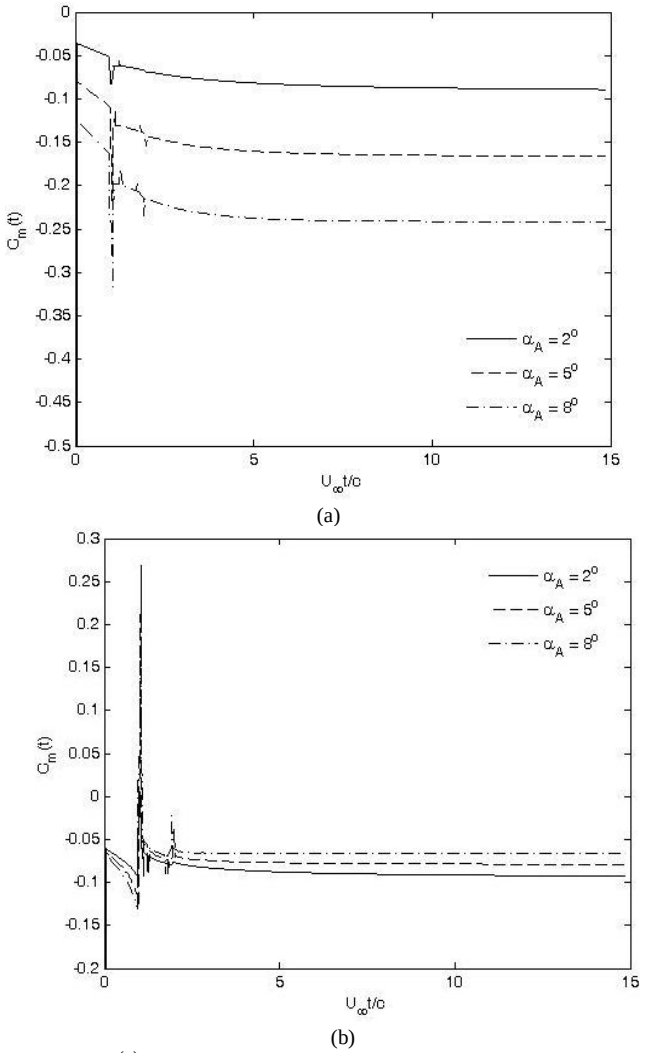

(a)

(b)

Fig. 21 $C_m(t)$ for $(X_0, Y_0) = (2c, 0)$, $V_A = V_B = 27$m/s, $\alpha_B = 4^o$ (a) airfoil A and (b) airfoil B

As explained earlier, this is due to the upwash created on the trailing airfoil by the trailing vortex shed from the leading airfoil, which is of a very high strength. The effect of this upwash vanishes as the vortex moves downstream and crosses the leading edge of the trailing airfoil.

No significant roll-up of the vortices shed from the leading airfoil **A** is observed but considerable roll-up is obtained for the trailing airfoil **B** as seen in Fig. 23. A prominent secondary roll-up is also seen for airfoil B.

Hence, the wake of the leading airfoil is significantly affected by the presence of the trailing airfoil.

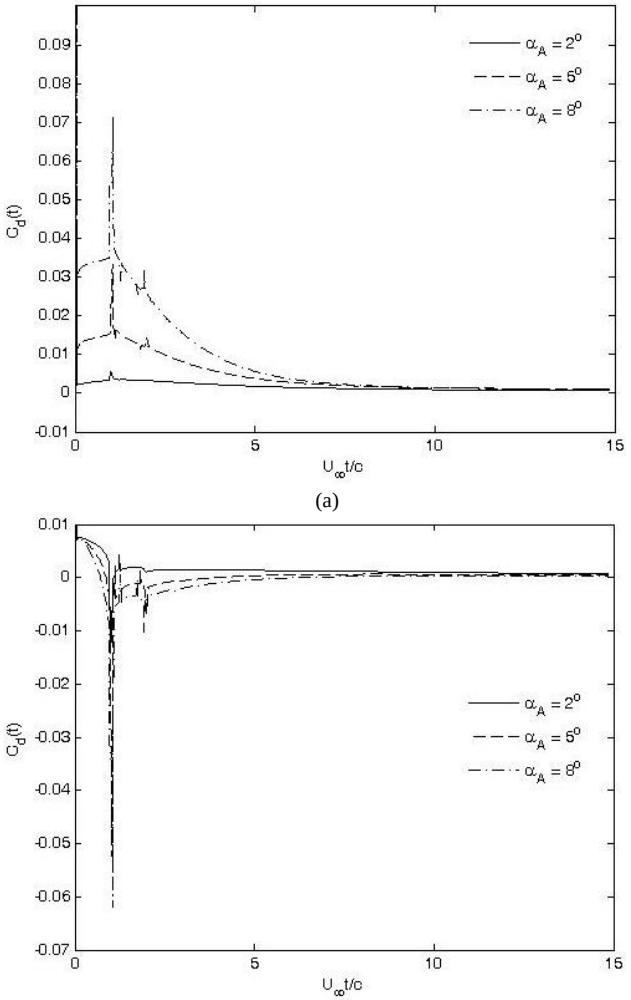

(a)

(b)

Fig. 22 $C_d(t)$ for $(X_0, Y_0) = (2c, 0)$, $V_A = V_B = 27$m/s, $\alpha_B = 4^o$ (a) airfoil A and (b) airfoil B

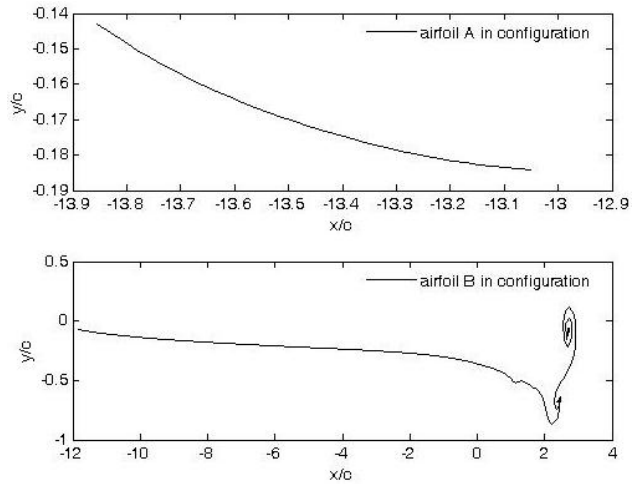

Fig. 23 Wake shape for $(X_0, Y_0) = (2c, 0)$ $V_A = V_B = 27$m/s, $\alpha_A = 8^o$, $\alpha_B = 4^o$

F. $C_d(t)/C_l(t)$ *Results*

In the unsteady analysis carried out in this work, it is observed that the aerodynamic characteristics of an airfoil operating alone is different from the case when it is

operating in configuration with another airfoil.

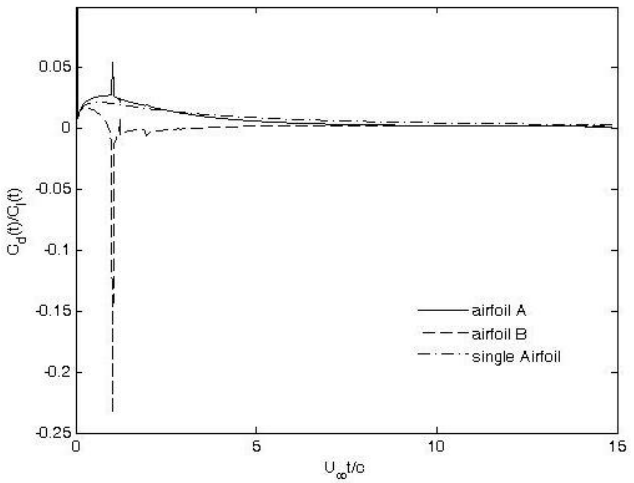

Fig. 24 sec B and C: $(X_0, Y_0) = (2c, 0)$ $V_A = V_B = 27$m/s, $\alpha_A = \alpha_B = 4^o$

Various results to emphasize this point have been presented in this paper and the reasons cited were explained in lieu of airfoil-airfoil and airfoil-vortex interactions.

It is seen that due to the "*disappearance*" or "*breaking-up*" of the vortices according to the near-field vortex-solid surface interaction, significant roll-up of the wake vortices from the leading airfoil is not obtained. This is deemed to be a viable physical result in terms of flow-physics.

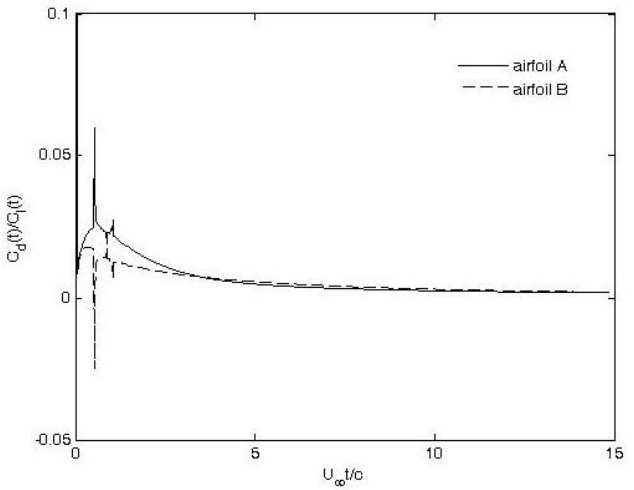

Fig. 25 sec D: $(X_0, Y_0) = (2c, 0.5c)$ $V_A = V_B = 27$m/s, $\alpha_A = \alpha_B = 4^o$

In this section we take a look at the variation of $C_d(t)/C_l(t)$ with $U_\infty t/c$ for sections B-E to make a statement on the possible gains of a formation flight regime in terms of reduced induced drag.

The effect of change in spatial offsets, X_0 and Y_0 on $C_d(t)/C_l(t)$ is shown in Figs 24 and 25. Fig. 24 shows the variation of $C_d(t)/C_l(t)$ for the two airfoils in configuration for a positive X_0 offset of 2c compared to when either of them is operating singly. Fig. 25 shows the same variation for the airfoils in configuration with a positive Y_0 offset of 0.5c. These values of X_0 and Y_0 are chosen since they produce the maximum peaks. The effect of temporal change, i.e change in α_A on $C_d(t)/C_l(t)$ is shown in Fig. 26.

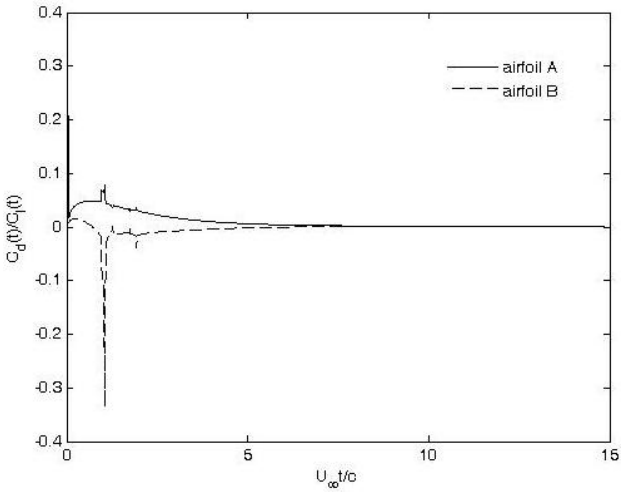

Fig. 26 sec E: for $(X_0, Y_0) = (2c, 0)$ $V_A = V_B = 27$m/s, $\alpha_A = 8^o$, $\alpha_B = 4^o$

The peak values of $C_l(t)$ and $C_d(t)$ for sections B-E are also tabulated in TABLE 1. The % relative changes are calculated according to the formula given in Equ. 6 and Equ. 7.

$$\frac{C_l(t)_i - C_l(t)_{single}}{C_l(t)_i} \times 100 \qquad \text{(Equ. 6)}$$

$$\frac{C_d(t)_i - C_d(t)_{single}}{C_d(t)_i} \times 100 \qquad \text{(Equ. 7)}$$

Where *i*= airfoil A or B in the configuration

From Table 1, it is seen that amongst the peak values, for the case when $Y_0 = +0.5c$ (sec D), for airfoil B, for a decrease in its $C_l(t)$ of ~33% there is a corresponding decrease in its $C_d(t)$ of ~ 200%. For the same case for airfoil A on the other hand, for an increase in its $C_l(t)$ of ~20% there is a corresponding increase in its $C_d(t)$ of ~ 70%. It is seen that this case gives the best results in terms of a trade-off between decrease in $C_l(t)$ and decrease in $C_d(t)$ for airfoil B and a decrease in $C_l(t)$ and increase in $C_d(t)$ for airfoil A among all the cases of airfoils A and B in configuration considered here.

References

[1] Seiler, P., Pant, A. and Hedrick, K. "*Analysis of bird formations"*, (2002) Proceedings of 41st IEEE Conference on Decision and Control, Las Vegas, Nevada, USA, December.

[2] Poore, S. O., Sanchez-Heiman, A. and Goslow, G. E. Jr., "Aircraft upstroke and evolution of flapping flight", (1997) Nature, Vol 387, pp 799-802, June.

[3] Steven Hoa, Hany Nassefa, Nick Pornsinsirirakb, Yu-Chong Taib, Chih-Ming Hoa, "Unsteady aerodynamics and flow control for flapping wing flyers", (2003) Progress in Aerospace Sciences, 39, 635–681.

[4] Bangash, Z. A., Sanchez, R. P. and Ahmed, A., "Aerodynamics of Formation Flight, Journal of Aircraft", (2006) Vol 43, No. 4, pp 907-912, July-August.

[5] Vachon M., Ray R., Walsh K., Ennix, K., "F/A-18 Aircraft Performance Benefits Measured During the Autonomous Formation Flight Project", (2002) AIAA 2002-4491, Aug.

[6] Bowles R. G. A. and Smith F. T., "Lifting multi-blade flows with interaction", (2000) J. Fluid Mech., vol. 415, pp. 203-226.

[7] D. Fanjoy, and D. J. Dorney, "A study of tandem-airfoil interaction in different flight regimes," (1997) AIAA 97-0515.

[8] L. Zannetti, F. Gallizio, and G. M. Ottino, "Vortex motion in doubly connected domains," (2008) J. Fluid Mech., vol. 612, pp. 143 – 152.

[9] Z. Husain, M. J. Abdullah, and T. C. Yap, "Two-dimensional analysis of tandem/staggered airfoils using computational fluid dynamics," International Journal of Mechanical Engineering Education 33/3.

[10] Katz, J. and Plotkin, A., *Low-speed Aerodynamics*, 2001, Cambridge University Press.

[11] A. J. Chorin, and P. S. Bernard, "Discretization of a vortex sheet, with an example of roll-up," J. of Computational Physics., vol. 13, No. 3, 1973.

[12] A. Fage and F. C. Johansen, "On the flow of air behind an inclined flat plate of infinite span" (1927) Proc. Roy. Soc. A 116, 170.

[13] T. Nakagawa, "On Unsteady Airfoil-Vortex Interaction", (1988) ACTA MECHANICA 75, 1-13.

[14] H. Wagner, "Uber die Entstehung des Dynamischen Autriebes von Tragflugeln", (1925) *Z.F.A.M.M*., Vol. 5, No. 1, pp 17-35.

[15] J. Katz and D. Weihs, "Behaviour of vortex wakes from oscillating airfoils", (1978) *J. Aircraft*, Vol. 15, No. 12.

[16] Max F. Platzer, Kerrin S. Neace and Chung-Kiang Pang, "Aerodynamic analysis of flapping wing propulsion", (1993) 31st Aerospace Sciences Meeting and Exhibit, AIAA 93-0484.

TABLE 1

$C_l(t)$ AND $C_d(t)$ PEAK/TROUGH RESULTS FOR CASE STUDIES B-E

Airfoil	SINGLE		IN FORMATION				% relative change in $C_l(t)$		% relative change in $C_d(t)$	
			A		B		A	B	A	B
	$C_l(t)$	$C_d(t)$	$C_l(t)$	$C_d(t)$	$C_l(t)$	$C_d(t)$				
Sec B	0.403	0.008								
Sec C (X_o = 2c)	-	-	0.469	0.025	0.250	-0.058	14.1	-61.2	68	-113.8
Sec D (Y_o= .5c)	-	-	0.5	0.030	0.303	-0.008	19.4	-33.00	73.3	-200
Sec E (α_A=8°)	-	-	0.901	0.071	0.185	-0.062	52.3	-117.8	88.7	-112.9